1 Reduced deuterium retention in self-damaged tungsten exposed to high-flux plasmas at high surface temperatures

M.H.J. 't Hoen[1], M. Mayer[2], A.W. Kleyn[1,3], H. Schut[4] and P.A. Zeijlmans van Emmichoven[1]

[1] FOM institute DIFFER, Association EURATOM-FOM, Partner in the Trilateral Euregio Cluster, PO Box 1207, 3430 BE Nieuwegein, The Netherlands
[2] Max-Planck-Institut für Plasmaphysik, Boltzmannstraße 2, D-85748 Garching, Germany
[3] University of Amsterdam, Science Park 904, NL-1098 XH Amsterdam, the Netherlands
[4] Delft University of Technology, Mekelweg 15, NL-2629 JB Delft, the Netherlands

Abstract

We investigated the effect of surface temperature on deuterium retention in self-damaged tungsten exposed to high-flux deuterium plasmas. The retention saturates at a W^{4+} fluence of about $3 \times 10^{17}\,m^{-2}$ and is strongly reduced for the present high surface temperatures of 800–1200 K as compared to previous experiments at 470–525 K. Combination of nuclear reaction analysis (NRA), thermal desorption spectroscopy and positron annihilation Doppler broadening (PADB) was used to investigate the reduction in deuterium retention. The NRA showed a strong reduction of retention at the surface at high surface temperatures. The PADB measurements suggest that during plasma exposure defects are mobile and cluster into larger clusters containing up to a few tens of vacancies. Tritium Migration Analysis Program 7 simulations show that trapping and de-trapping rates are very high for defects with trapping energies below $\sim$1.5 eV. The strong reduction in retention seems to be caused by the reduced amount of mono-vacancies and small vacancy clusters in combination with their strong depopulation due to thermal trapping and de-trapping.[1]

Published in:
Nuclear Fusion **53** 043003 (2013)

1.1 Introduction

Tungsten is foreseen as divertor material in future magnetic fusion devices such as ITER. Its good thermal properties such as high thermal conductivity, its high melting point and low erosion rate make tungsten favourable over other materials. For safety and efficiency reasons, it has been decided that the tritium inventory should be kept below 700 g [1]. It is therefore important to understand the effect of high-flux hydrogen plasmas on the material in detail. The solubility of hydrogen isotopes in tungsten is low. However, continuous bombardment with 14.1 MeV neutrons degrades the material properties and introduces damage, which may act as a trap site for hydrogen.

Hydrogen isotope retention in neutron-irradiated tungsten was studied in [2–4]. Since neutron irradiation is very time-consuming, MeV range heavy ions have frequently been used to simulate neutron damage. Previously, high-energy ion bombardment was found to increase the deuterium retention [5–7] and the deuterium concentration in the damage zone reaches 1.4 at.% [8]. This concentration was measured at surface temperatures below 550 K, where vacancies are not mobile. However, the divertor is predicted to operate at temperatures of around 600–1300 K [9]. In this study, the focus is on the influence of elevated surface temperatures on deuterium retention in self-damaged tungsten. Damage in tungsten was created by pre-irradiation with 12.3 MeV W ions.

The damage cascade of a high-energy ion has a complicated structure. The process of damage creation has been discussed in many papers, for example the book by Was [10] gives a good overview. A high-energy ion entering the lattice transfers part of its energy to atoms, the so-called primary knock-on atoms (PKA's). These PKA's cause further collisions cascades. Molecular dynamics simulations of these cascades have been carried out by several research groups to determine the amount and size of the vacancies and vacancy clusters that are created. Guinan and Kinney [11] showed that due to intra-cascade recombination in the cool-down phase of the damage cascade, the amount of initially produced defects is reduced. Caturla *et al* [12] used the recoil spectra of 1.9 GeV protons and simulated the damage evolution with kinetic Monte Carlo to investigate the cascade efficiency for the production of defects and their size distribution. They found large recovery of the damage during the cool-down phase. The remaining defect type was dominated by mono-vacancies and interstitials, only few clusters consisting of 2–3 vacancies and 2–4 interstitials were found. Troev *et al* [13] performed numerical calculations of damage in tungsten irradiated by fusion neutrons. They also show formation of mono-vacancies, di-vacancies, a few vacancy clusters, interstitials and small number of interstitial clusters containing more than three atoms. Fikar *et al* [14] studied the influence of different tungsten inter-atomic potentials on the amount and type of radiation damage. No important difference in the defect production was found. In all cases, mostly mono-vacancies were produced. The rest of the defects (35%) formed mainly small clusters, the maximum cluster size was about 35 vacancies. The probability for clustering and the size of the largest clusters tend to increase with increasing PKA energy [15]. Note that TEM studies show that in addition to vacancies also large numbers of dislocation loops are formed during irradiation [16].

Eleveld and van Veen [17] used positron annihilation techniques to study the effect

of stepwise heating on the damage in tungsten induced by 15 keV deuterium ions. They found that vacancy clustering takes place at ∼650 K and argue that the clusters have sizes of four to ten vacancies. Further cluster growth proceeded in two stages. At ∼1050 K the initially formed clusters broke up and formed clusters with 11–16 vacancies. These vacancy clusters disappeared at around 1450 K in favour of clusters containing 40–60 vacancies. Finally, these clusters were removed by annealing above 1700 K.

In this paper, we have studied the effect of temperature on deuterium retention in self-damaged tungsten at temperatures up to 1200 K. The results will be discussed in terms of the diffusion of deuterium in tungsten, trapping and de-trapping from vacancies and vacancy clusters, and the mobility of vacancies.

1.2 Experiment

The work presented was performed with the same experimental techniques as described in [8], but with a three times higher power input. Briefly, the polycrystalline tungsten materials (99.96% purity) were provided by PLANSEE and annealed for 1 h at 1273 K prior to implantation. The cleanliness of the targets was checked by X-ray photoelectron spectroscopy (XPS) before and after plasma exposure. Material damage was created by W^{4+} ions with kinetic energy of 12.3 MeV. The 3 MV tandem ion accelerator at IPP-Garching irradiated an implantation area of 12 mm in diameter, homogeneously, at normal incidence and at room temperature. Damage levels were calculated by SRIM [18] using the average value of 90 eV for the displacement threshold energy as reported by [19]. Varying the ion irradiation time resulted in peak damage levels of up to 0.45 displacements per atom (dpa). These peak damage levels are used as reference for our experiments. Damage profiles extend up to 1.5 µm depth. The damage rate at which the targets were damaged was $(3 \pm 1) \times 10^{-4}\,\mathrm{dpa\,s^{-1}}$.

All targets were implanted with deuterium at similar plasma conditions in the linear plasma generator Pilot-PSI [20]. The damaged targets have been exposed to four 20 s plasma pulses in an axial magnetic field of 0.8 T. Thomson scattering measurements were used to determine the electron density and electron temperature of the plasma beam [21]. The shape of the plasma beam is approximately Gaussian with an electron density of $9.0 \times 10^{20}\,\mathrm{m^{-3}}$ in the centre and a full width half maximum of about 14 mm. The maximum electron temperature of 1.6 eV was measured in the centre of the beam. The targets were electrically floating during plasma exposure. Assuming that the ion temperature equals the electron temperature and using the Bohm criterion [22], the peak deuterium ion plasma flux is calculated to be $5.6 \times 10^{24}\,\mathrm{m^{-2}s^{-1}}$. Temperature profiles of the surface of the target were measured with a fast infrared camera (FLIR SC7500-MB). The maximum surface temperature was 1250 K at the beginning of the plasma pulse; during the 20 s plasma pulse this decreased to 1150 K. The profiles of the surface temperature of the target averaged over the plasma pulse and of the flux are shown in figure 1.1. The target was indirectly cooled via a water cooled copper block which was very effective; after switching off the plasma, the temperature of the targets was back to room temperature within typically 1 s.

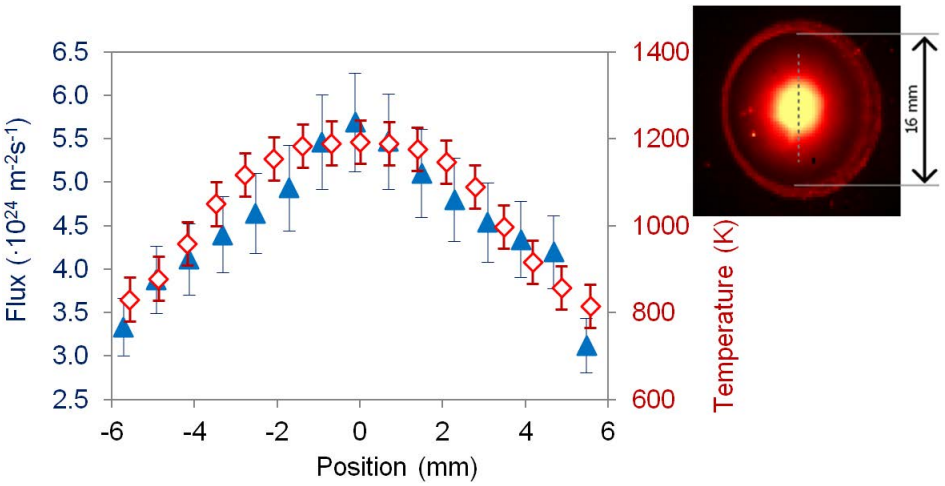

Figure 1.1: Radial dependence of the plasma flux (solid triangles) and average surface temperature (open diamonds). The insert shows a typical infrared image of the W sample during plasma exposure.

Deuterium depth profiles were measured by nuclear reaction analysis (NRA) at IPP-Garching four weeks after plasma exposure by using the nuclear reaction D(^{3}He, p)^{4}He [23, 24]. Radial scans were made by positioning the ^{3}He beam spot of 1 mm in diameter at seven locations on the targets. The energy was scanned from 690 keV to 4.0 MeV at each position, so that the deuterium concentration could be measured down to 6 µm depth. The measured proton energy distributions were used to determine the depth profiles of the retained deuterium by use of the SimNRA program [25].

After NRA, about eight weeks after plasma exposure, the total deuterium retention and the desorption temperature peaks of the deuterium were determined by thermal desorption spectroscopy (TDS). With a ceramic heater, the tungsten samples were heated with a linear temperature ramp of 1 K/s to 1273 K. A Balzers QMA125 Quadrupole Mass Spectrometer (QMS) monitored the mass 4 (D_2) and mass 3 (HD) signals in the residual gas in the chamber, to determine the total amount of deuterium released from the target during the temperature ramp. The absolute sensitivity was determined using calibrated leaks of H_2 and D_2. For the sensitivity of the mass 3 signal, the average of the sensitivities of mass 2 and mass 4 was taken. Mass 19 and 20, respectively HDO and D_2O, were also detected. Qualitative analysis showed that these signals did not significantly exceed the background values.

Positron annihilation Doppler broadening (PADB) was used to monitor formation and clustering of defects [26, 27]. The annihilation reaction of an electron with a positron produces two gammas, each with an average energy of 511 keV. As a consequence of momentum conservation, the momentum of the electron-positron pair results in a Doppler broadening of the 511 keV annihilation energy. A typical measurement of the gamma spectrum can be found in the insert of figure 1.7. The S (sharpness) parameter is calculated as the ratio of counts registered in a fixed central electron momentum window ($|p_{\|}| < 3.5 \times 10^{-3} m_0 c$) to the total number of counts in the photon peak. This choice of mo-

mentum window makes the S parameter sensitive to annihilations with low momentum valence electrons and implies that the S parameter is relatively high for a defect rich material: for a positron trapped in an open volume defect (such as a dislocation, a monovacancy or a vacancy cluster) the probability for annihilation with a valence electron is enhanced at the cost of annihilation with a core electron. Similarly, the W (wing) parameter is obtained from the high momentum regions W_{left} and W_{right} ($10 \times 10^{-3} m_0 c < |p_\parallel| < 26 \times 10^{-3} m_0 c$) and accounts for annihilations with high momentum core electrons. Therefore, the W parameter is relatively high for a defect-free material. In conclusion, as a function of defect concentration the behaviour of S and W parameter is opposite.

In this study, the PADB experiments were performed with the Delft Variable Energy Positron beam (VEP). Positrons emitted from a ^{22}Na source were, after moderation to thermal energies and subsequent acceleration, injected in the samples with a kinetic energy from 0.1 to 25 keV. The beam intensity is about 10^4 positrons per second, the beam diameter at the target 8 mm. The mean implantation depth of the positrons, $\langle z \rangle$, scales with the implantation energy according to $\langle z \rangle \; A/\rho \times E^{1.62}$ [28]. Here, A is the material independent parameter ($4 \times 10^{-5} \mathrm{kg\,m^{-2}keV^{-1.62}}$), ρ is the sample density ($\mathrm{kg\,m^{-3}}$) and E is the positron implantation energy (keV). For tungsten, the positron energy of 25 keV corresponds to an implantation depth of about 400 nm.

To investigate the effect of temperature on the radiation damage in tungsten, the temperature evolution of the S and W parameters of four samples were monitored with PADB during several annealing stages. These samples were prepared in the following way. First, all samples were annealed for 1 h at 1273 K. Then, two of these tungsten samples were pre-irradiated with W^{2+} ions with a kinetic energy of 5.5 MeV. One of these pre-irradiated samples was subsequently exposed to deuterium plasma in Pilot-PSI to implant deuterium. Also, one of the two non-damaged samples was exposed to deuterium plasma. The kinetic ion energy of 5.5 MeV was used for pre-irradiation, so that in the tungsten material only a shallow region of 600 nm with a maximum at 250 nm was damaged. This range is close to the range covered by the PADB measurements. Deuterium plasma exposure was performed at a peak electron density of $2 \times 10^{20}\,\mathrm{m^{-3}}$ and a maximum electron temperature of about 0.6 eV. The surface temperature was chosen at about 520 K, in order to stay below the temperature where vacancies become mobile. Next, all four samples were vacuum annealed to the indicated temperatures in figure 1.6, followed by PADB measurements after each heating step. All S and W parameters reported here, are normalized with respect to almost defect-free tungsten (heated for 24 h at 1800 K).

1.3 Results

1.3.1 X-ray Photoelectron Spectroscopy (XPS)

Before plasma exposure, tungsten (10%), carbon (40–60%) and oxygen (20–40%) were observed with XPS. XPS typically probes the top $\sim$10 nm of a W sample. As discussed in [8] oxygen and carbon form a native layer of a few nanometer on top of tungsten, when

stored under ambient conditions. This layer will be removed during the initial stages of plasma exposure. Similar amounts of tungsten, carbon and oxygen were observed after plasma exposure. In addition, the surfaces contained calcium and fluorine concentrations up to 6% and boron with a maximum concentration of 10.5%.

The boron concentration decreased with the time that the source was in operation, i.e., targets exposed at a later moment contained less impurities. A decrease in boron content of a factor of 2 was found between the first and the last sample. The self-damaged samples were exposed to plasma in random order with respect to the level of damage. No effect on the D retention of the order of exposure was observed. E.g. the shape of the saturation curves is smooth and similar as in previous experiments while the amount of boron is reduced with a factor two. From this, we conclude that boron and other impurities did not have a significant effect on the amount of retained deuterium. It is predominantly determined by the damage level and not by the sequence in which the samples were exposed.

1.3.2 Nuclear reaction analysis

We investigated our targets with NRA to get information on the local depth distribution of the retained deuterium. Measurements were carried out at different positions on the target: 0, 1, 3 and 6 mm from the centre, which were exposed at temperatures of respectively 1195, 1185, 1050 and 800 K and plasma fluxes of 5.6, 5.4, 4.5 and 3.2 $\times 10^{24}\,\mathrm{m^{-2}s^{-1}}$. The integrated amount of deuterium retained in the top 6 µm of the sample as function of radial position is shown in figure 1.2. The amount strongly depends on the radial position as well as on the pre-irradiation damage. In the centre, where temperature and flux are maximal, the retention is minimal.

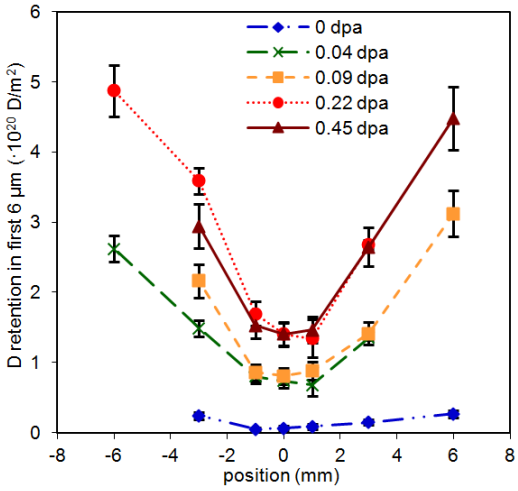

Figure 1.2: Radial dependence of the total retained deuterium as function of measurement position at the target.

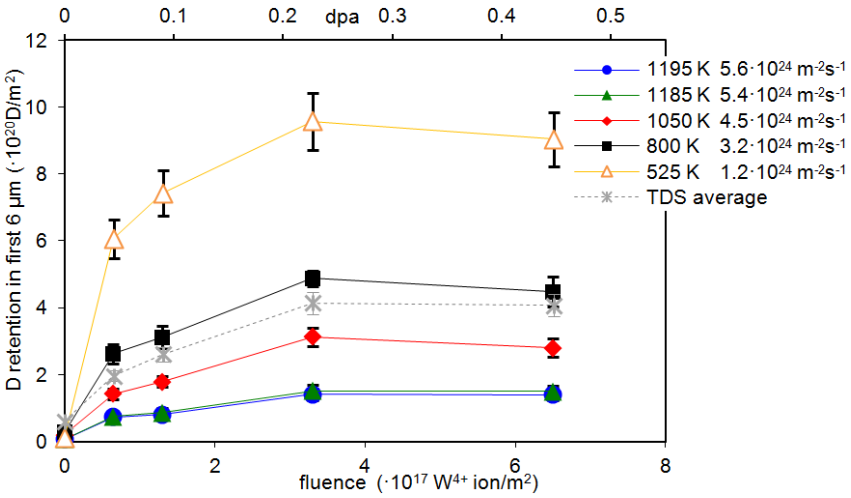

Figure 1.3: D retention saturates as function of W^{4+} pre-irradiation fluence. The solid points show the D retention at different positions of the targets. The open triangles are data [8] from a tungsten target exposed at 525 K. The dotted line marked with stars show the total integrated TDS signal divided by the area damaged by pre-irradiation.

The integrated amount of retained deuterium as function of pre-irradiation fluence is shown in figure 1.3. For comparison, the results of our previous experiments at a surface temperature of 525 K, the low temperature regime, are also plotted [8]. It is clear that the present results, like the previous ones, show saturation at the damage level of about 0.25 dpa. The D retained in the W targets from the present high surface temperature exposures is drastically lower than in the low temperature regime.

The measured NRA depth profiles are shown in figure 1.4. The measured amount of deuterium increases with pre-irradiation damage. For all samples, the D depth profiles show a strong reduction in the centre of the target, where particle fluxes and surface temperatures are highest. In the near-surface layer (<0.5 µm) the reduction is in particular strong.

The reduction in the D retention in the centre of the target is most likely related to the local high surface temperature. An increase of particle flux of the deuterium implantation would not lead to a decrease of particles stored in the tungsten. The reduction in retention may be the result of the high trapping and de-trapping rates at these high surface temperatures, which would reduce the fraction of defects that are filled with deuterium. We studied this possibility with TMAP7, a one-dimensional transport code. Another possible explanation could be that the mobility of defects at these elevated temperatures results in removing and clustering of defects. This may lead to a reduction in retention as well. PADB was used to collect information on the defect behaviour as a function of the surface temperature.

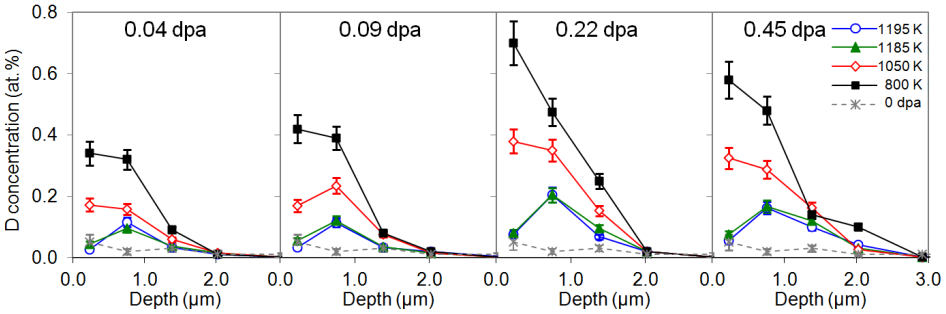

Figure 1.4: Depth distributions of the deuterium, retained in damaged tungsten targets, pre-irradiated to (a) 0.045, (b) 0.09, (c) 0.22 and (d) 0.45 dpa. The shown D depth profiles were measured at four spots on the target: in the centre (1195 K, $5.6 \times 10^{24}\,\mathrm{m^{-2}s^{-1}}$), 1 mm off-centre (1185 K, $5.4 \times 10^{24}\,\mathrm{m^{-2}s^{-1}}$), 3 mm off-centre (1050 K, $4.5 \times 10^{24}\,\mathrm{m^{-2}s^{-1}}$) and 6 mm off-centre (800 K, $3.2 \times 10^{24}\,\mathrm{m^{-2}s^{-1}}$). The dotted line with asterisk symbols show the D depth profile in the undamaged tungsten target.

1.3.3 Thermal desorption spectroscopy

In figure 1.5, the TDS results are shown for the damaged targets. For comparison, the result for a damaged target exposed to plasma at lower surface temperature [8] is displayed. Virtually no difference is observed between the 0.22 dpa and 0.45 dpa samples. This shows that the tungsten material is saturated with defects at 0.22 dpa. The undamaged sample (0 dpa) shows the contribution of the deuterium trapped in intrinsic traps and damage created during the plasma exposure itself. As compared to our previous results obtained at the low surface temperature exposure, the desorption peak at low temperature ($\sim$550 K) is strongly reduced and has shifted to higher temperatures. The high temperature peak has shifted from 880 K to 975 K and has become narrower.

For high temperature exposure cases, the TDS signal is dominated by the deuterium released from the periphery region of the sample. Not only did we find that the local deuterium retention at 6 mm distance from the centre a factor 3–4 higher than in the centre (figure 1.2), the area of the periphery is large compared to the central region.

1.3.4 Positron annihilation Doppler broadening

With PADB, we investigated the behaviour of the defects as function of temperature in a qualitative way. Figure 1.6 shows the measured S parameter as a function of positron energy of the sample that was pre-irradiated with 5.5 MeV W^{2+} ions (without any plasma exposure). The measured S parameter distributions are also shown after heating the sample to the temperatures as indicated in figure 1.6.

To determine the material specific S parameter of almost defect-free tungsten, a sample was recrystallized by heating for 24 h to 1800 K (shown in figure 1.6 by the red stars). Detailed VEPFIT (Variable Energy Positron fit) [29] analysis of the change in S parameter as function of implantation energy, yields a positron diffusion length of

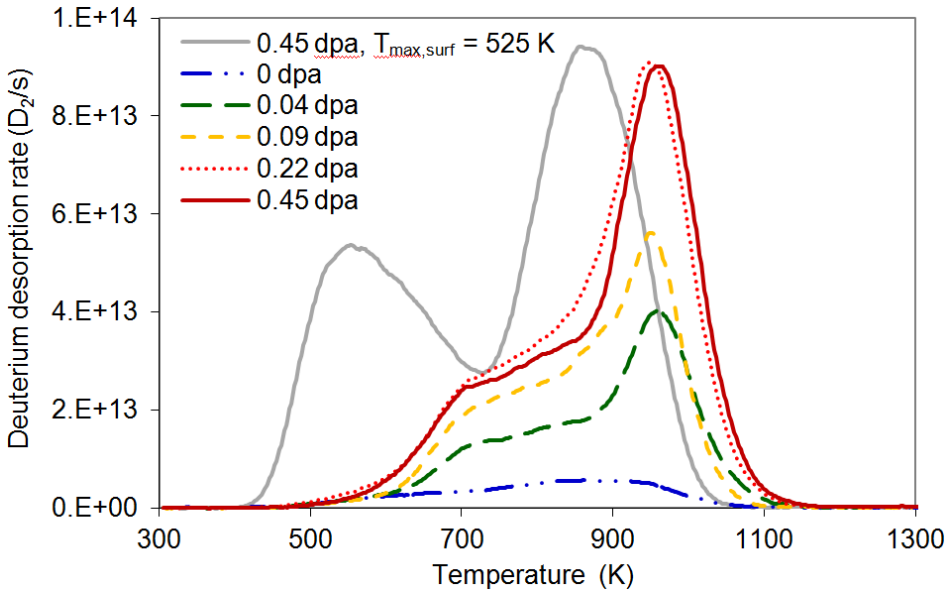

Figure 1.5: TDS mass 4 (D_2) signal. The temperature was ramped at a speed of 1 K/s. For comparison, the results from the low temperature exposure [8] are plotted as a solid line.

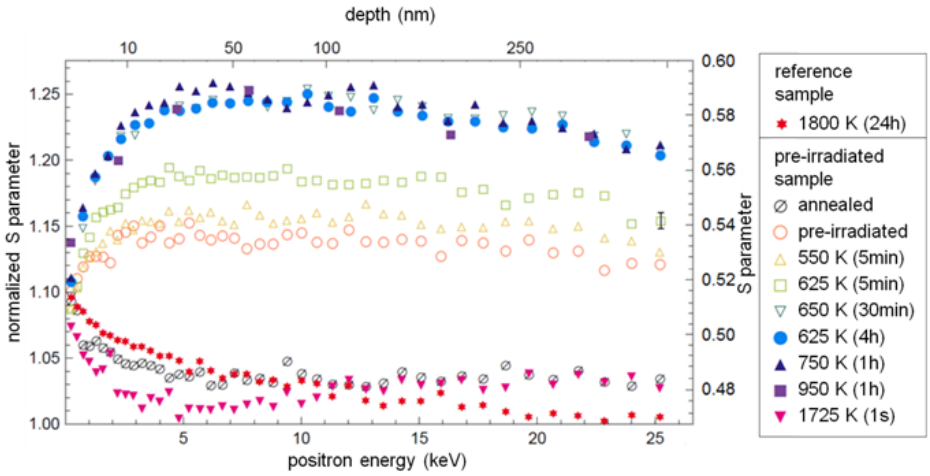

Figure 1.6: The *S* parameter versus positron energy after different annealing stages of the target that was irradiated with 5.5 MeV W^{2+} ions. Before irradiation the target was annealed for 1 h at 1273 K. For comparison, the *S* parameter distributions for a recrystallized target (24 h at 1800 K) with very low defect density are also shown. On the second *x*-axis the average implantation depth is given according to the Makhov distribution.

about 100 nm and an *S* parameter bulk value of 0.468. This value was used for normalization. The observed gradual change of *S* parameter from the surface value ($S_{surface}$) at low positron energy towards the bulk value (figure 1.6) at high-energy is due to the energy dependent broadening of the positron implantation profile (straggling) and diffusion of positrons after stopping and thermalization.

The normalized S_{bulk} parameter of the annealed sample is 1.04 (figure 1.6, ∅). The 4% higher *S* value readily shows that the annealed sample still contains defects that effectively trap positrons. This is confirmed by the small positron diffusion length of 15 nm, found by VEPFIT analysis, which is well below the above-discussed value of 100 nm for defect-free tungsten. The elevated *S* value is typical for positrons trapped at defects.

After pre-irradiation with MeV ions, the normalized *S* parameter in the damaged regime increases to a value of up to 1.14 (figure 1.6, ○). As discussed in [17], such an *S* parameter indicates the presence of additional small vacancy clusters generated in the material due to the ion irradiation. By heating the target for 5 min at 550 and 625 K, the *S* parameter increases to a value of up to 1.19. Further increase of *S* to 1.25 is observed after heating of the target at 650 K for 30 min. This increase of *S* is an indication for the growth of vacancy clusters. Subsequent heating steps of 4 h at 625 K, 1 h at 750 K and 1 h at 950 K, did not cause any further change in the *S* parameter. This indicates that the vacancy clusters were stable and did not significantly change in size [30]. As a final step, the target was heated for a short time to 1725 K after which the measured *S* parameters dropped to values close to those of the annealed target. This means that vacancy clusters became mobile and were removed from the material. Note that the measured *S* parameters agree very well to the results from Eleveld *et al* [17]. Obviously, although the damage was created in a different way, i.e., high-energy tungsten ion damage (our work) versus high-energy deuterium ion implantation [17], the defects and their temperature behaviour are rather similar.

Without any lattice defects, a material exhibits characteristic *S* and *W* values. As discussed in the experimental section, introduction of defects increases *S* and decreases W. It is instructive to plot the normalized *S* parameters of our samples against the normalized *W* values (the *W* values were also normalized to the values found for defect-free tungsten). The *SW* plot with data points of all samples is given in figure 1.7. Each data point shown consists of the average *S* and *W* parameters in the positron implantation energy range of 5–10 keV. We chose this range because at smaller implantation energies, the surface affects the *S* and *W* values. At higher implantation energies, positrons annihilated beyond the damaged range contribute to the signal. The *SW* defect-free point is also indicated in figure 1.7.

Annealed tungsten, without pre-irradiation, has a normalized *S* parameter of about 1.05 and a normalized *W* parameter of about 0.78. Increasing the temperature in steps, as indicated in figure 1.6 and determining the *S* and *W* parameters shows a linear change in the *S* and *W* parameters towards the values for defect-free tungsten. This linear behaviour indicates the presence of defects and their removal by the heating steps [31]. Due to the heating less defects are available, so that the positrons will annihilate predominantly with tungsten core electrons. The *SW* point (1.14, 0.6) for tungsten after pre-irradiation with MeV ions is also indicated in figure 1.7. Upon heating with similar heating steps to

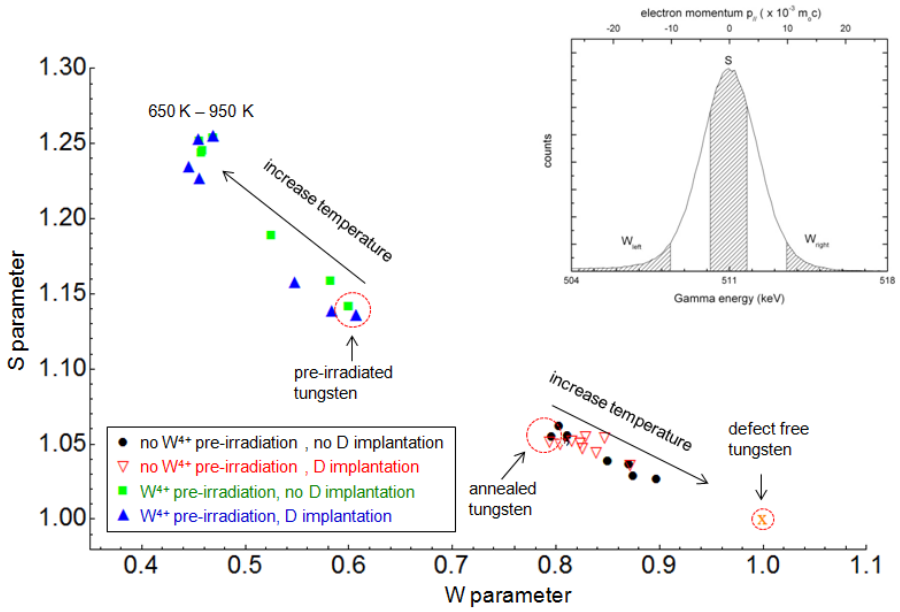

Figure 1.7: Plot of the *SW* values of the four samples after the different heating steps mentioned in figure 1.6. The samples irradiated with MeV W^{4+} ions and non-irradiated samples react in an opposite way to heating up to 950 K. The insert shows a typical gamma energy distribution resulting from positron-electron annihilations, the definition of *S* and *W* parameters is marked by the hatched areas.

950 K, the behaviour is opposite from that of the non-irradiated targets. The *S* parameter increases up to a value of about 1.25 (at 950 K) and the *W* parameter decreases to about 0.46. After briefly heating to 1725 K, the *SW* measurements points of the pre-irradiated samples end up close to the defect-free *SW* point (not shown in figure 1.7). Additionally, note that the differences between plasma-exposed and unexposed targets are small. The deuterium implanted in the tungsten did not influence the PADB results.

The observed increase in *S* parameter for the pre-irradiated target can be explained by either the increase of defect concentration or the growth of formation of vacancy clusters. As the irradiation produced defect concentration is above the thermal equilibrium concentration, the more likely explanation for the increase in *S* parameter is the growth of vacancy clusters. The opposite behaviour of pre-damaged and non-damaged targets in the *SW* plot would then be explained by the difference in initial defect density. At low initial defect density, the defects have a high probability of reaching the surface or grain boundaries and anneal. In the pre-irradiated targets, in other words at high defect density, the defects are more likely to form larger clusters. These clusters are stable at higher temperatures. The change in slope of the irradiated and non-irradiated targets also strengthens the difference in type of defects involved.

1.3.5 Simulations with TMAP7

TMAP7 is a program to simulate diffusion and trapping of hydrogen in materials. An elaborate description of the code is given in [32]. TMAP7 was used to simulate the diffusion during the implantation process of deuterium by plasma exposure at a flux of $4 \times 10^{24}\,\mathrm{m^{-2}s^{-1}}$ and the desorption of deuterium by ramping the temperature. Diffusion and solubility values of hydrogen in tungsten from Frauenfelder [33] were used. The tungsten material was separated into 64 depth layers, with a thickness varying from 2.5 nm at the surface to 1 µm at the backside.

Trapping and de-trapping rates are strongly dependent on the temperature. To investigate its effect on the D retention, we used the following approach. First, the TDS results presented in [8], were fitted with TMAP7. These results were obtained at lower surface temperature exposures (below 525 K), where defects were not mobile. In the fits, flat damage profiles up to 1.25 µm depth were assumed and the trapping energies and absolute vacancy densities were varied until reasonable agreement with the experiments was obtained. The results were then used as an input parameter for simulation of the diffusion during implantation at higher temperatures, thereby initially assuming that the defect distribution was not affected.

In figure 1.8, the TMAP7 simulation of the TDS profile together with the experimental results from 0.22 dpa LTR is shown (dashed grey line). In the fit three types of traps were used, the first with a trapping energy of 1.2 eV and a density of 0.5 at.%, the second with a trapping energy of 1.4 eV and a density of 0.2 at.% and the third with a trapping

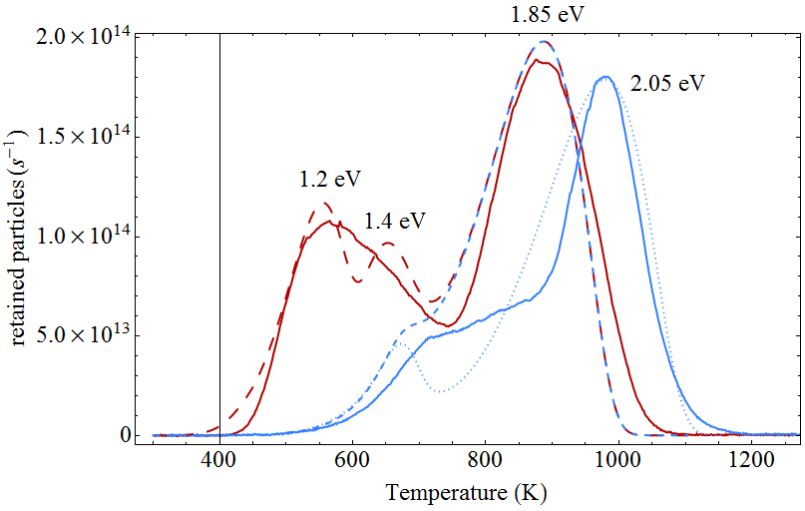

Figure 1.8: The solid lines show the experimental TDS results. The low surface temperature (0.22 dpa) is plotted in grey and the high temperature TDS profile (0.22 dpa) in black. The dashed and dotted lines are the results from the TMAP7 simulations of the TDS profile. For the low temperature regime three traps were assumed up to a depth of 1.25 µm: 1.2 eV, 1.4 eV and 1.85 eV with a trap density of respectively 5×10^{-3}, 2×10^{-3} and 7×10^{-3}. Implantation of the same damage profile at 1000 K results in the dashed black desorption profile. The shift of the high temperature peak could only be fitted by choosing a trapping energy of 2.05 eV (dotted line)

Table 1.1: Fraction of retained particles at four different temperatures for three trapping energies.

surface temperature (K)	1.2 eV	1.4 eV	1.85 eV
500	100%	100%	100%
800	63%	97%	100%
1000	5.0%	35%	99%
1200	0.5%	3.4%	73%

energy of 1.85 eV and a density of 0.7 at.%. The densities were chosen such that the total defect density adds up to the experimentally observed 1.4 at.% [8]. Here, we assume one D atom per defect. Implantation of deuterium at higher temperatures reduces the fraction of D-filled defects of all three defects, because de-trapping takes place. This is illustrated in table 1.1.

The TDS profile of the TMAP7 run for an implantation temperature of 1000 K is shown figure 1.8 (dashed black line). This temperature is approximately the average temperature of the targets during implantation at high temperatures (HTR). Indeed, the low temperature peak significantly decreases as result of the strong depopulation of the traps at 1.2 and 1.4 eV. The intensity of the high temperature peak does not decrease. However, in the experiment the high temperature peak is located at significantly higher temperatures than in the simulations. Running TMAP7 again and increasing the 1.85 eV trapping energy to 2.05 eV, led to the result shown by the dotted black curve. In this simulation, the peak at about 975 K agrees quite well with the experiments. In the temperature range of 700–850 K some intensity seems to be 'missing'. The reason may be that the actual trapping energies are most likely not strictly defined, but rather characterized by a broader distribution. TMAP7 cannot correctly represent such a distribution. It may also be that mono-vacancies and/or small vacancy clusters are still present in the target during the experiments, but not taken into account in the simulations.

It should finally be noted that we have also simulated the desorption of deuterium during the 1 s cool down phase as possible cause for the reduction in retention. This did not lead to any significant desorption of deuterium. During the exposure most of the deuterium is released (99.95%), only a factor 1×10^{-6} of the deuterium is retained in the material.

1.4 Discussion

As discussed in [8], the saturation of D retention as a function of pre-irradiation W ion fluence for targets exposed to plasmas at surface temperatures up to 525 K is caused by saturation of damage creation in the pre-irradiation phase. The same holds for targets exposed to plasmas at higher surface temperatures (800–1200 K). However, the maximum amount of retained deuterium is significantly reduced (figure 1.3). The NRA results in figure 1.2 clearly show that the surface temperature plays an important role. We have used NRA, TDS, positron annihilation techniques, and TMAP7 simulations to understand this reduced D retention in more detail.

The PADB experiments presented in figure 1.6 yield information on the defects in tungsten. Directly after pre-irradiation, the *S* parameter has increased up to 14% above the defect-free reference value. It was discussed in [17] that this *S* parameter indicates creation of additional vacancies and vacancy clusters. This is in line with MD simulations on irradiation damage in materials: Caturla *et al* [12] and Fikar *et al* [14] have shown that for an average PKA energy of ∼17 keV, the value we estimated using SRIM for 12.3 MeV W^{4+} ions, significant amounts of defects are produced.

In the TDS spectrum for the targets exposed to plasma at low surface temperatures up to 525 K (figure 1.8), two distinct peaks were observed. Heinola *et al* [34] have shown with density-functional theory calculations that a mono-vacancy can hold up to six hydrogen atoms. The corresponding trapping energies range from 1.6 eV for the first atom down to 1.2 eV for the fifth atom and 0.64 eV for the sixth. These values are in the range of what we found for the TDS peak at low temperature (∼550 K), which suggests that deuterium trapped in mono-vacancies contributes to this peak. It should be noted that deuterium trapped in dislocations, which is not taken into account in our simulations, may also contribute to this low temperature peak. As discussed in the introduction, irradiation of materials with the MeV range ions also creates small vacancy clusters. The desorption peak at higher temperatures (∼880 K) may be related to deuterium trapped in such small clusters, either in atomic or molecular form.

The behaviour of defects with temperature was studied with PADB. In the PADB experiments, the targets were subsequently heated in steps, initially leading to an increase in the *S* parameter. After heating for 30 min at 650 K, the normalized *S* parameter has increased to about 1.25. As discussed in the previous section, this increase in *S* is probably caused by the growth of vacancy clusters. According to [17], the clusters are thought to contain up to about ten vacancies. In further heating steps, the *S* parameter remained constant even after heating the target for 1 h at 950 K. Only after a brief heating step at 1725 K, the *S* parameter was significantly reduced.

During the plasma experiments at high surface temperatures the targets reached temperatures in the range of 800–1200 K. In this temperature regime, according to the PADB experiments, growth of vacancy clusters will take place during plasma exposure. The periphery region of the surface, i.e. with the lowest exposure temperatures, will contain clusters containing up to about ten vacancies (corresponding to a normalized *S* parameter of about 1.25 in the PADB experiments). These larger clusters have also formed in the centre area, exposed at higher temperatures up to 1200 K. Additionally, defects close to the surface were able to reach the surface and annihilate. This is supported by our NRA results. In figure 1.4, the strong reduction of deuterium retention in the surface region was measured.

This clustering of mono-vacancies and small vacancy clusters into larger clusters was confirmed by TDS. Apart from the significant decrease of the low temperature peak, a shift of the high temperature peak to ∼975 K was observed. According to the TMAP7 simulations, this high temperature peak corresponds to a trapping energy of 2.05 eV. This energy is close to the value of 2.1 eV that was interpreted by several others [6, 35, 36] as trapping of deuterium in voids. Ogorodnikova *et al* [37] report a trap energy of 1.84-2.34 eV from chemisorption of atomic D on the internal surface of a void. Interesting

was, that TMAP7 did not reproduce the fact that the measured high temperature peak was much narrower. To explain this, we need the NRA depth profiles from figure 1.4. Here, we found that the D retention in the surface region was strongly reduced. Retention of deuterium in a narrower damage profile will lead to a narrow peak in the TDS.

Our results suggest that during plasma exposure at high temperatures, mono-vacancies and small vacancy clusters are mobile and form larger clusters containing tens of vacancies. Some smaller clusters however also remain present, although their contribution to the retention is significantly less because of the strong depopulation of these lower energy traps at the used high temperatures. The amount of deuterium trapped in the larger clusters present in the high temperature exposures is similar to the amount in the smaller clusters as produced in the irradiation process and still present during low temperature plasma exposures. The strong reduction in retention observed at high temperature exposures, therefore, seems to be caused by the reduced amount of mono-vacancies and small clusters in combination with their strong depopulation due to thermal trapping and de-trapping. In addition, the number of dislocations are also expected to be strongly reduced after high temperature exposures.

1.5 Conclusion

We investigated the effect of surface temperature on D retention above the temperature where vacancies become mobile. The saturation behaviour of the retention that we observed for low temperature exposures and that originates in the pre-irradiation damage, is still present. The retention at these high surface temperatures is however strongly reduced. The reduction is strongest close to the surface. Our results suggest that the reduction in D retention is the result of both the reduced amount of mono-vacancies and small vacancy clusters and their reduced population due to thermal trapping and de-trapping. The PADB data on defect evolution in tungsten upon heat treatment indicated formation of vacancy clusters, which are stable at higher temperatures. The shift of the high temperature peak in the TDS spectrum can be explained by the clustering of mono-vacancies and small vacancy clusters into larger clusters. From TMAP7 simulations we found that depopulation due to thermal trapping and de-trapping is strong for traps with a low binding energy. The strong reduction of the D retention in the region close to the surface can be explained by the annealing of vacancies.

Acknowledgement

This work, supported by the European Communities under the contract of Association between EURATOM/FOM, was carried out within the framework of the European Fusion Program with financial support from NWO. The views and opinions expressed herein do not necessarily reflect those of the European Commission. The authors would like to thank R.S. Al for the technical support at Pilot-PSI, J. Dorner and M. Fußeder for the technical assistance with the ^{3}He beam analysis and E. Zoethout for the XPS analysis.

Bibliography

[1] J. Roth et al, *Recent analysis of key plasma wall interactions issues for ITER*, J. Nucl. Mater. **390-391** (2009) 1–9.

[2] M. Shimada et al, *First result of deuterium retention in neutron-irradiated tungsten exposed to high flux plasma in TPE*, J. Nucl. Mater. **415** (2011) S667–S671.

[3] M. Shimada et al, *The deuterium depth profile in neutron-irradiated tungsten exposed to plasma*, Phys. Scr. **2011** (2011) 014051.

[4] M. Shimada et al, *Overview of the US-Japan collaborative investigation on hydrogen isotope retention in neutron-irradiated and ion-damaged tungsten*, Fusion Eng. Des. **87** (2012) 1166–1170.

[5] B. Tyburska et al, *Deuterium retention in self-damaged tungsten*, J. Nucl. Mater. **395** (2009) 150–155.

[6] G. Wright et al, *Hydrogenic retention in irradiated tungsten exposed to high-flux plasma*, Nucl. Fusion **50** (2010) 075006.

[7] W. Wampler and R. Doerner, *The influence of displacement damage on deuterium retention in tungsten exposed to plasma*, Nucl. Fusion **49** (2009) 115023.

[8] M. H. J. 't Hoen et al, *Saturation of deuterium retention in self-damaged tungsten exposed to high-flux plasmas*, Nucl. Fusion **52** (2012) 023008.

[9] G. Federici, H. Wuerz, G. Janeschitz and R. Tivey, *Erosion of plasma-facing components in ITER*, Fusion Eng. Des. **61-62** (2002) 81–94.

[10] G. S. Was. *Fundamentals of radiation material science: Metals and Alloys*. Springer-Verlag, Berlin Heidelberg, New York (2007).

[11] M. Guinan and J. Kinney, *Molecular dynamic calculations of energetic displacement cascades*, J. Nucl. Mater. **104** (1981) 1319–1323.

[12] M. J. Caturla et al, *Multiscale modeling of radiation damage: applications to damage production by GeV proton irradiation of Cu and W, and pulsed irradiation effects in Cu and Fe*, J. Nucl. Mater. **296** (2001) 90–100.

[13] T. Troev, N. Nankov and T. Yoshiie, *Simulation of displacement cascades in tungsten irradiated by fusion neutrons*, Nucl. Instrum. Methods Phys. Res. B **269** (2011) 566–571.

[14] J. Fikar and R. Schaeublin, *Molecular dynamics simulation of radiation damage in bcc tungsten*, Nucl. Instrum. Methods Phys. Res. B **255** (2007) 27–31.

[15] J. Fikar and R. Schäublin, *Molecular dynamics simulation of radiation damage in bcc tungsten*, J. Nucl. Mater. **386-388** (2009) 97–101.

[16] T. Matsui, S. Muto and T. Tanabe, *TEM study on deuterium-irradiation-induced defects in tungsten and molybdenum*, J. Nucl. Mater. **283-287** (2000) 1139–1143.

[17] H. Eleveld and A. van Veen, *Void growth and thermal desorption of deuterium from voids in tungsten*, J. Nucl. Mater. **212-215** (1994) 1421–1425.

[18] J. F. Ziegler, M. D. Ziegler and J. P. Biersack, *SRIM-The stopping and range of ions in matter*, Nucl. Instrum. Methods Phys. Res. B **268** (2010) 1818–1823.

[19] ASTM E521-96. *Standard Practice for Neutron Radiation Damage Simulation by*

Charge-Particle Irradiation, Annual Book of ASTM Standards, Vol. 12.02. American Society for Testing and Materials, Philadelphia (1996).

[20] G. J. van Rooij et al, *Extreme hydrogen plasma densities achieved in a linear plasma generator*, Appl. Phys. Lett. **90** (2007) 121501.

[21] H. J. van der Meiden et al, *High sensitivity imaging Thomson scattering for low temperature plasma*, Rev. Sci. Instrum. **79** (2008) 013505.

[22] D. Bohm. *The Characteristics of Electrical Discharges in Magnetic Fields, chapter 3*. ed A Guthrie and R K Wakerling (NewYork: McGraw-Hill) (1949).

[23] V. K. Alimov, M. Mayer and J. Roth, *Differential cross-section of the D(^{3}He,p)^{4}He nuclear reaction and depth profiling of deuterium up to large depths*, Nucl. Instrum. Methods Phys. Res. B **234** (2005) 169–175.

[24] M. Mayer, E. Gauthier, K. Sugiyama and U. von Toussaint, *Quantitative depth profiling of deuterium up to very large depths*, Nucl. Instrum. Methods Phys. Res. B **267** (2009) 506–512.

[25] M. Mayer. SIMNRA User's guide, Report IPP 9/113, Max-Planck-Institut für Plasmaphysik, Garching (1997).

[26] H. Schut, *A variable energy positron beam facility with applications in materials science*, PhD Thesis, Delft University of Technology, Delft (1990).

[27] A. van Veen, *Positron beam analysis techniques and gas desorption spectrometry for the characterization of defects in materials*, J. Trace Microprobe Tech. **8** (1990) 1–29.

[28] A. Vehanen, K. Saarinen, P. Hautojärvi and H. Huomo, *Profiling multilayer structures with monoenergetic positrons*, Phys. Rev. B **35** (1987) 4606–4610.

[29] A. van Veen et al, *Positron beams for solids and surfaces*, Am. Inst. Phys. Conf. Proc. **218** (1990) 171–196.

[30] A. van Veen et al, *Hydrogen exchange with voids in tungsten observed with TDS and PA*, J. Nucl. Mater. **155-157** (1988) 1113–1117.

[31] A. Debelle, M. Barthe and T. Sauvage, *First temperature stage evolution of irradiation-induced defects in tungsten studied by positron annihilation spectroscopy*, J. Nucl. Mater. **376** (2008) 216–221.

[32] G. R. Longhurst. TMAP7 User Manual. Technical report, INEEL/EXT-04-02352 (Idaho: Idaho National Engineering and Environmental Laboratory) (2004).

[33] R. Frauenfelder, *Solution and Diffusion of Hydrogen in Tungsten*, J. Vac. Sci. Technol. **6** (1969) 388–397.

[34] K. Heinola and T. Ahlgren, *First-principles study of H on the reconstructed W(100) surface*, Phys. Rev. B **81** (2010) 073409.

[35] M. Poon, A. Haasz and J. Davis, *Modelling deuterium release during thermal desorption of D^+-irradiated tungsten*, J. Nucl. Mater. **374** (2008) 390–402.

[36] M. Fukumoto et al, *Deuterium trapping in tungsten damaged by high-energy hydrogen ion irradiation*, J. Nucl. Mater. **390-391** (2009) 572–575.

[37] O. V. Ogorodnikova, J. Roth and M. Mayer, *Ion-driven deuterium retention in tungsten*, J. Appl. Phys. **103** (2008) 034902.